# In situ infrared spectroscopic ellipsometry as a tool to probe the formation of sol–gel based mesoporous films

Hajar Amyar, Caroline Byun, Mondher Besbes, Andrea Cattoni, Heinz Amenitsch, Cédric Boissiere, Marco Faustini

# In situ infrared spectroscopic ellipsometry as a tool to probe the formation of sol-gel based mesoporous films

*Hajar Amyar,[1,2] Caroline Byun,[1] Mondher Besbes,[2] Andrea Cattoni,[3], Heinz Amenitsch,[4] Cédric Boissiere,[1] Marco Faustini[1,5*]*

***Author information***

*1 Sorbonne Université, CNRS, Laboratoire Chimie de la Matière Condensée de Paris (LCMCP), F-75005 Paris, France*

*2 Université Paris-Saclay, Institut d'Optique Graduate School, CNRS, Laboratoire Charles Fabry, 91127 Palaiseau, France*

*3 Centre de Nanosciences et de Nanotechnologies (C2N), CNRS UMR 9001, Université Paris-Saclay, Palaiseau, France.*

*4 Institute of Inorganic Chemistry, Graz University of Technology, Graz, Austria*

*5 Institut Universitaire de France (IUF), 75231 Paris, France*

*marco.faustini@sorbonne-universite.com*

**Abstract**

Probing the formation of sol-gel mesoporous films and characterizing them under environmental/in-operando conditions represents an important challenge to optimize their performances. Obtaining a complete picture of the system usually requires a combination of multiple techniques. In this work, we introduce in situ infrared (IR) ellipsometry equipped with an environmental chamber as a tool to follow simultaneously the evolution of structural, optical and chemical properties during the formation of sol-gel derived mesoporous films. As a case study, we investigate the formation of mesoporous $TiO_2$ by comparing a conventional thermal treatment and a low-temperature annealing by UV irradiation. In both cases, the structural optical and chemical evolution could be monitored during the IR ellipsometric experiment. Interestingly, UV-annealing allows the fabrication of mesoporous $TiO_2$ films at low temperatures enabling the formation of plasmonic mesoporous composites. At last, we critically discuss the advantages and drawbacks of IR ellipsometry for in situ investigations compared to conventional UV-visible ellipsometry by providing additional insights for future developments.

**Keywords**

ellipsometry, coatings, titania, annealing, plasmonic

**Graphical Abstract**

Using Infrared ellipsometry to probe the structural, optical and chemical evolution during the formation of sol-gel derived mesoporous films

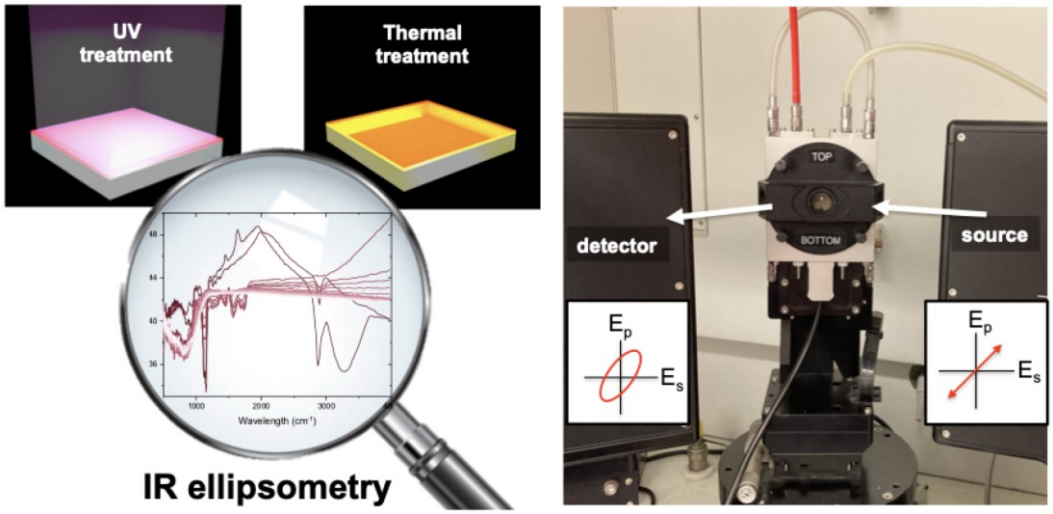


Highlights

- IR ellipsometry is used to characterize the formation of $TiO_2$ based mesoporous films
- Structural, optical and chemical evolutions can be investigated during thermal or UV treatments
- UV-annealing is well suited to fabricate composite plasmonic mesoporous films

## 1) Introduction

Sol-gel based porous films find applications in many technological relevant domains[1] including optics and photonics,[2-4] photocatalysis for air depollution,[5,6] electronics and data storage,[7-12] energy (catalytic layers, solar cells),[13-16] sensing (selective adsorption)[17,18] or separation (membrane).[19] Probing the formation of porous films and characterizing them under environmental/in-operando conditions represents an important challenge from both fundamental and applicative points of view.[20]

In an ideal case, the measurement itself needs to be non-destructive, time-resolved and compatible with environmental chambers (at ambient/high pressure, controlled temperature, liquid medium, under flux, etc). Often obtaining a complete picture of the evolution of systems in the presence of external stimuli[21] requires a combination of multiple techniques[22,23] and different experiments that often can't be performed in comparable conditions. In addition, the choice of the technique strongly depends on the characteristic scale of the porous system (micro-meso-macro). While a universal technique doesn't exist, some methods exhibit good potential in terms of versatility under environmental conditions; for instance, UV-visible spectroscopic ellipsometry is probably the most powerful characterization method to probe the formation and the properties of optical films.[24-26] Briefly, the technique consists of (i) measuring the change in polarization of light reflected by a surface and (ii) applying optical models to determine the refractive index dispersion $n(\lambda)$ and the thickness $h$ of the films. Since the measurement is fast and non-destructive, it allows the determination of $n(\lambda)$ and *thickness* vs time under controlled atmosphere,[17,27] temperature,[28] irradiation,[29] liquid biological media[30] (and combinations of these). Notably, the so-called “Environmental Ellipsometric Porosimetry” (EEP) was developed to fully characterize the porosity, the mechanical properties and the sorption properties of micro and mesoporous films (sol-gel based and MOFs).[31-34] Despite the versatility of the technique, one main limitation can be mentioned. While the spectral range of the typical UV-visible-NIR ellipsometry (200-1700 nm) enables probing structural evolution (thickness and optical constants), nothing can be said about the chemical evolution of the materials. Recent progress in infrared ellipsometric technology allow now combining the optical sensitivity and versatility of UV-visible spectroscopic ellipsometry with the chemical sensitivity of FTIR spectroscopy. Covering a very wide spectral range in the IR, through a single measurement, multiple parameters can be investigated. In addition to structural and optical parameters, the chemical composition can be determined by IR absorption at high resolution. For instance, standard IR ellipsometry was used to quantify the residual water in silica films. [35] Moreover, more recent IR ellipsometric set-up can be interfaced with environmental chambers with controlled temperature and atmosphere. By taking advantage of such

advances, herein we introduce Infrared Ellipsometry equipped with an environmental chamber (with controlled atmosphere and temperature) as an emerging "multifunctional" tool to probe the formation of sol-gel mesoporous films. We study the formation of highly porous mesoporous $TiO_2$ as a case study. More specifically, we compare the formation of mesoporous $TiO_2$ films obtained by conventional thermal treatment [36] and by UV irradiation; this latter photo-annealing is conducted at room temperature to meet the important requirement to integrate $TiO_2$ on thermally sensitive materials (such as plastics or plasmonic nanostructures) or to develop new inorganic resists for photolithography. In addition, this study is complemented by additional characterization including environmental UV-Visible-Near-Infrared ellipsometry, SEM, and GI-SAXS. At last, as proof of concept of application, the thermal and photo-annealed mesoporous $TiO_2$ were applied onto gold bipyramid nanoparticles to obtain plasmonic mesoporous composite layers. Hyperspectral microscopy in dark-field mode was used to probe the effect of the different annealing method of the $TiO_2$ films on the plasmonic response of single objects, opening interesting perspectives for sensing applications.

## 2) Materials and methods

**2.1 Chemical solution.** The precursor solution of the mesoporous $TiO_2$ film was fabricated through a typical sol-gel chemical method using amphiphilic block copolymers as template agents. Pluronic F127 purchased from Sigma-Aldrich was first dissolved in an ethanolic solution under continuous stirring. Then $TiCl_4$ diluted with EtOH with a molar ratio of 1:5 (used as the inorganic source) was added into the solution dropwise, followed by further stirring for a few hours to ensure homogeneity before using the solution.[5] The molar ratios used for this study are 1:0.018:47:11 for $TiCl_4$:F127:EtOH:$H_2O$.

**2.2 Film fabrication.**

The films were deposited on silicon substrates by spin coating with 3500 rpm/min for 20s at room temperature and ambient relative humidity of 21°C and 45%. For the in-situ IR ellipsometric measurements we used platinum-coated silicon wafer that are more reflective in the IR region. For the photo-annealing process, the film was treated using Dymax ECE 5000 flood UV-lamp curing systems at different exposure times. The lamp irradiates the samples in the range in the UV range between 280 and 315nm.

**2.3 Characterization** After coating, films were directly placed and characterized with a UV-visible-NIR Woollam spectroscopic Ellipsometer (SE) (from 240 to 1700nm) and IR-Vase Ellipsometer covering a range from 1.7 to 30 microns (333 to 5900 $cm^{-1}$). Both ellipsometers are equipped with a programmable heating stage (-80°C to 600°C) and an environmentally controlled chamber in which the local environment of the films can be controlled in terms of

relative humidity. Data measurement and analyses were performed with CompleteEASE and WVASE software for the UV-vis and IR ellipsometry, respectively. The porosity and the sorption response of the mesoporous titania films were evaluated using ellipsometric thermo porosimetry. Adsorption-desorption isobars were obtained by following the evolution of optical constants and thickness when varying the temperature of the heating stage and keeping a constant relative humidity on the chamber ($P/P_0$). A mass flow controller is used to manage the water $P/P_0$ by combining two gas flows: (i) dry air flow with solvent $P/P_0$ ($H_2O$)=0, and (ii) air flow that has gone through a bubbler containing liquid water to obtain a saturated vapor $P/P_0$($H_2O$)=1. The structural properties of the films were determined and compared with GISAXS measurements using a synchrotron radiation source and SEM. The GISAXS analysis were performed at the Austrian SAXS beamline at the ELETTRA synchrotron in Trieste (Italy) at a photon energy of 8 keV.[37] The beam size was set to 1x0.2 $mm^2$ (HxV). SAXS images were collected in grazing incidence (0.236°) using a Pilatus3 1M detector (Dectris AG, Switzerland) at a distance of 1942.3 mm from the sample. SEM imaging was performed on a SU-70 Hitachi FESEM. The extinction spectra of plasmonic nanoparticles and spectral mapping were acquired by a CytoViva hyperspectral scanning system with a spectrometer (30 mm slit width, spectral range: 400– 1000 nm) using reflection dark-field 10x or 100x objectives. Hyperspectral images were acquired with an acquisition time of 0.50 s in air.

## 3) Results

### 3.1 IR ellipsometry to probe formation of $TiO_2$ mesoporous films

The fabrication scheme of the mesoporous $TiO_2$ based films is illustrated in Figure 1. The films are obtained from solutions containing the Ti precursors (chlorides) and, a block-copolymer Pluronic F127. A typical protocol to obtain highly ordered mesoporous films requires an F127/Ti molar ratio of 0.005 [38,39]. Instead, we employs here a larger organic/inorganic ratio of 0.018 to obtain $TiO_2$ films with higher porous volume (typically >30%) and lower refractive index.[6] The films are applied on silicon substrates coated with a platinum layer (to enhanced the reflectivity in the IR range) by spin-coating.[14] After deposition, the films are processed by two methods: a thermal annealing and a photo-curing by UV-lamp The goal is to decompose the organic template and condensate the $TiO_2$ network. IR ellipsometry is thus ideally suited to investigate the phenomena occurring during these annealing processes (decomposition, shrinkage, etc). The study is complemented by analyses carried out by UV-visible-NIR ellipsometry to confirm the results. The structure and porosity of the final films are then investigated by scanning electron microscopy, GI-SAXS and ellipsometric (thermo) porosimetry.

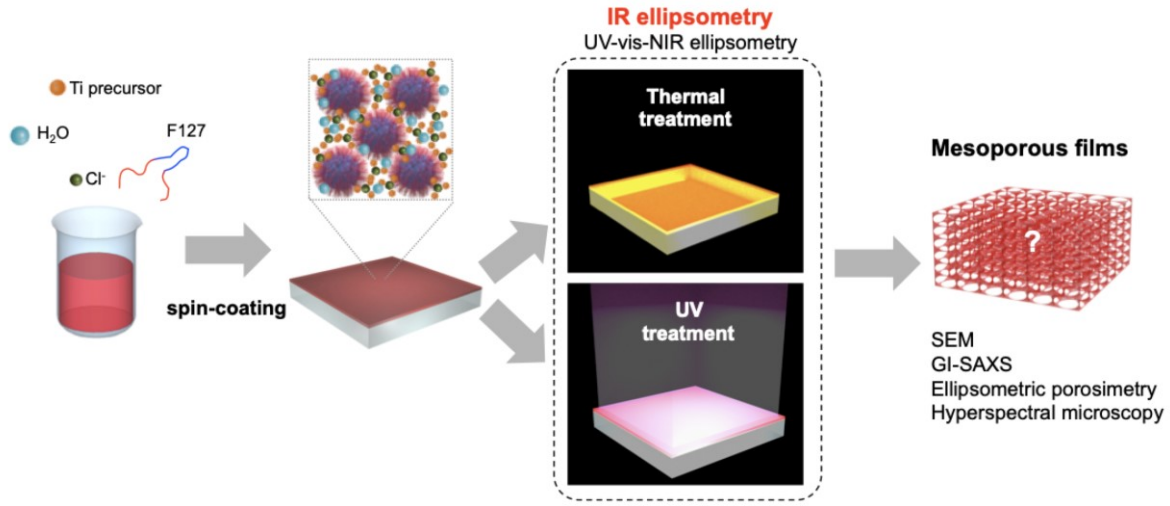


***Fig. 1*** *Fabrication scheme of the block-copolymer-templated $TiO_2$ mesoporous films: starting from a solution, a hybrid film is obtained by spin-coating on silicon substrates. The final mesoporous films are obtained though two annealing methods that are investigated by IR ellipsometry: thermal treatment or UV treatment*

The core technique of this study is spectroscopic ellipsometry. During an ellipsometric experiment, a polarized light beam interacts with the film. Changes in polarization of the reflected beam are parametrized by the interference amplitude component Ψ and the phase difference Δ. The Ψ and Δ curves are then fitted with optical models to determine the thickness and the optical constants: refractive index (n) and the extinction coefficient (k) as a function of the wavelength. Both UV-visible and IR ellipsometries provide evolution of n, k as a function of the wavelength and thickness. However, by IR ellipsometry, Ψ and Δ curves present absorptions due to vibrational modes, providing a way to follow the evolution of the chemical composition of the films. Ellipsometric analysis is not destructive and can be used for environmental analysis. In the present study, the ellipsometric study was performed in an environmental chamber which enables control the atmosphere and temperature, as shown in the photograph in Figure 2.

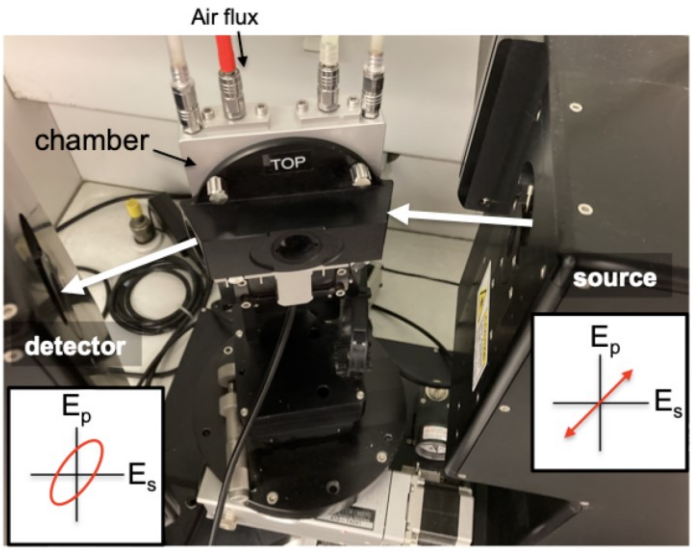


***Fig. 2*** *Photograph of the IR ellipsometric set-up*

We first investigated the optical constant of the hybrid film after spin-coating (and before annealing). The measurement was taken in the closed chamber in dry air (RH<10%) to avoid uncontrolled water uptake from the ambient humidity. From an ellipsometric measurement we obtain Ψ and Δ curves that need to be fitted to determine the optical constants and the thickness. Due to the presence of multiple absorption peaks in the IR range, our fitting procedure is done in two steps. Figure 3(a) shows the Ψ and Δ curves in the range 3500-5500cm$^{-1}$ a "transparent", non-absorbing region. The curves are thus fitted by Cauchy dispersion to obtain an accurate value of thickness (1310 nm in this case). This is an important step to obtain the value of n and k in the absorbing regions. Once the thickness is obtained, one can determine the optical constants (n and k) for the entire IR range by using B-spline parametrization,[40] a convenient mathematical fitting of the dielectric function as show in Figure 3(b). The n curve shown in Figure 3(c) presents a background value around 1.5, not surprising considering the high loading of polymer. The values of thickness and the refractive index were also confirmed by UV-vis-NIR ellipsometry. As shown in Figure 3(d) the k curves show several peaks that are associated with vibrational bands of the chemical species in the hybrid film. The curve shows many different features. The strong band at ca. 1100 cm$^{-1}$ can be mainly attributed to the C-O-C stretching in both PEO and PPO [41] [42] overlapping other contributions such as C–C stretching (1150 cm$^{-1}$) and $CH_2$ rocking (1060 cm$^{-1}$). The large O-H stretching band at 3200-3400 cm$^{-1}$ partially overlaps in the range 2850-2920 cm$^{-1}$ with the $CH_2$ symmetric and antisymmetric stretching bands of Pluronic F127.[43] The attribution of the two peaks below 950 cm$^{-1}$ is not straightforward. These contributions at lower wavenumber can be likely attributed to Ti oxoclusters present in the films after evaporation.

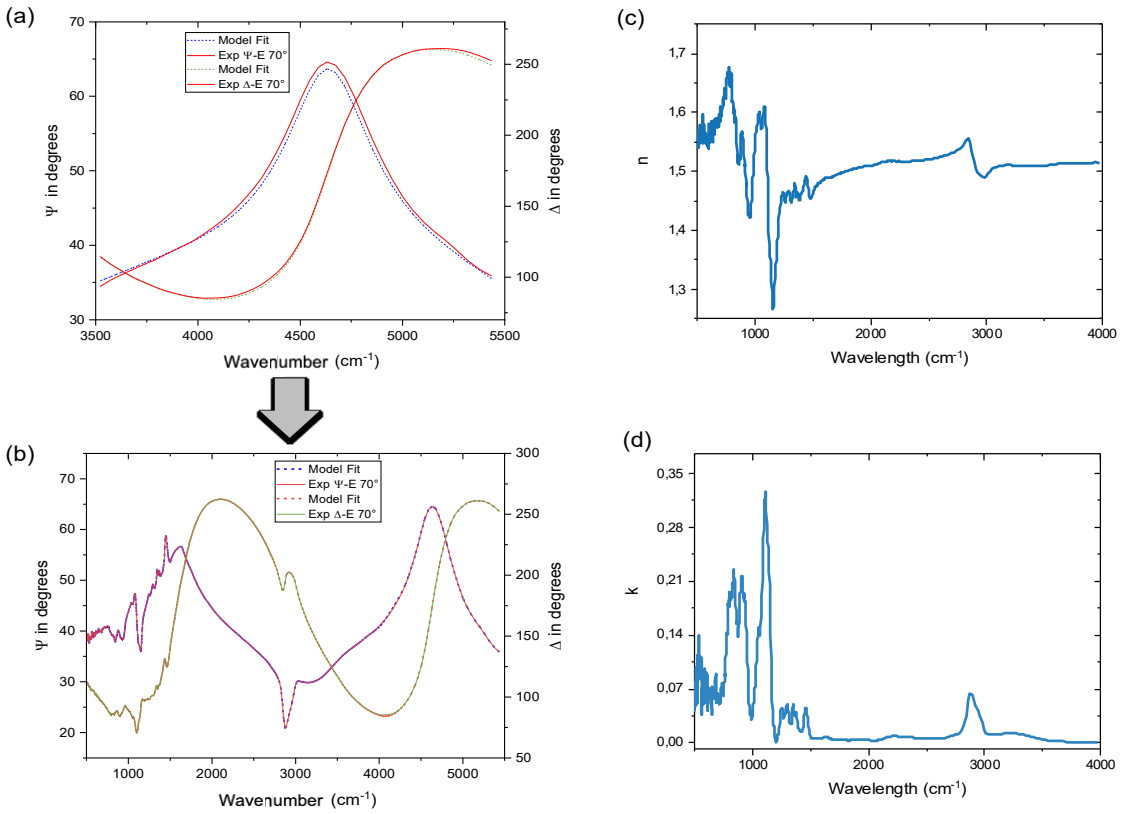


***Fig. 3*** Ψ and Δ experimental and fitted curves *obtained by IR ellipsometry on the hybrid film before annealing in (a) the non-absorbing region (to determine the thickness) and in (b) the full range. Evolution of (c) the refractive index and (d) extinction coefficient of the film before annealing.*

### 3.2 IR ellipsometric study of thermal annealing

We first investigated the effect of thermal annealing by using the in-situ IR ellipsometry set-up shown in Figure 2. The in situ ellipsometric measurements were performed by increasing the temperature in the chamber from 25°C up to 500°C in air. Calcination at this temperature results in crystalline mesoporous materials composed of $TiO_2$ anatase. [36] Figure 4 (a and b) present the evolution of Ψ and Δ curves of the film for increasing temperatures. The curves present oscillations due to constructive interferences generated at the substrate-film-air interfaces. In addition, typical signatures of vibrational absorption are also visible. By employing the methodology described above we fitted the curves to obtain the thickness and then n and k. The evolution of the normalized thickness as a function of the temperature is shown in Figure 4(c). As expected, the film contracts during thermal treatment due to the loss of volatile species and of the polymer decomposition. Figure S1 shows the evolution of n as a function of the temperature. The variation in the background values (in the non-absorbing ranges) are attributed to variation in optical density of the film during decomposition of the

organic template (or inorganic condensation) that can be better studied by analyzing the evolution of k. In order to compare the n and k values, it is important to remember that n and k are dimensionless numbers characterizing the optical constants and the interaction of light in a given unit of volume. Since the volume of the films decreases during the experiment, the k curves must be multiplied by the thickness for each temperature. Figures 4(d and e) show the evolution of k multiplied by the thickness for increasing temperature by focusing in the ranges 950-1250 and 2700-3100 $cm^{-1}$ to follow the evolution of the C-O and C-H bands, respectively. Starting above 100°C, the peaks attributed to the block-copolymer progressively decrease in intensity with increasing temperature at relatively low temperature. This trend is unusual since the decomposition of the Pluronic F127 block-copolymer usually takes place at higher temperature (above 200°C).[5] However, it is also well established that PEO (and PPO) degradation proceeds by random chain scission of the C-O bond by thermally activated radical process already at temperature below 100°C.[44] Similar results were obtained in previous ex-situ FTIR studies[45] on block-copolymer templated $TiO_2$ films in which significant degradation occurs from 100 °C, as a consequence of the thermal fragmentation of the block copolymer. In addition, it has been reported that in the case of mesoporous $TiO_2$ films, the block-copolymer decomposition temperature can be lowered by decreasing the heating rate.[36] This is likely our case; since the acquisition time of each measurement is 30 minutes, we performed a step-by-step treatment with long calcination times (more than 7 hours) leading to a block-copolymer decomposition at lower temperatures. To verify that, we performed the same in situ experiment by UV-vis-NIR ellipsometry equipped with a thermal chamber that enable faster acquisition and heating rate (5°C $min^{-1}$ in this case). The evolution of thickness as a function of the temperature is reported in Figure S2. The thickness contraction curve in Figure S2 is similar to the curve obtained by IR ellipsometry (Figure 4c) in terms of general trend and absolute values. However, by applying a faster heat treatment (by UV-vis-NIR ellipsometry), the thickness contraction appears at higher temperature in agreement with previous findings.[36]

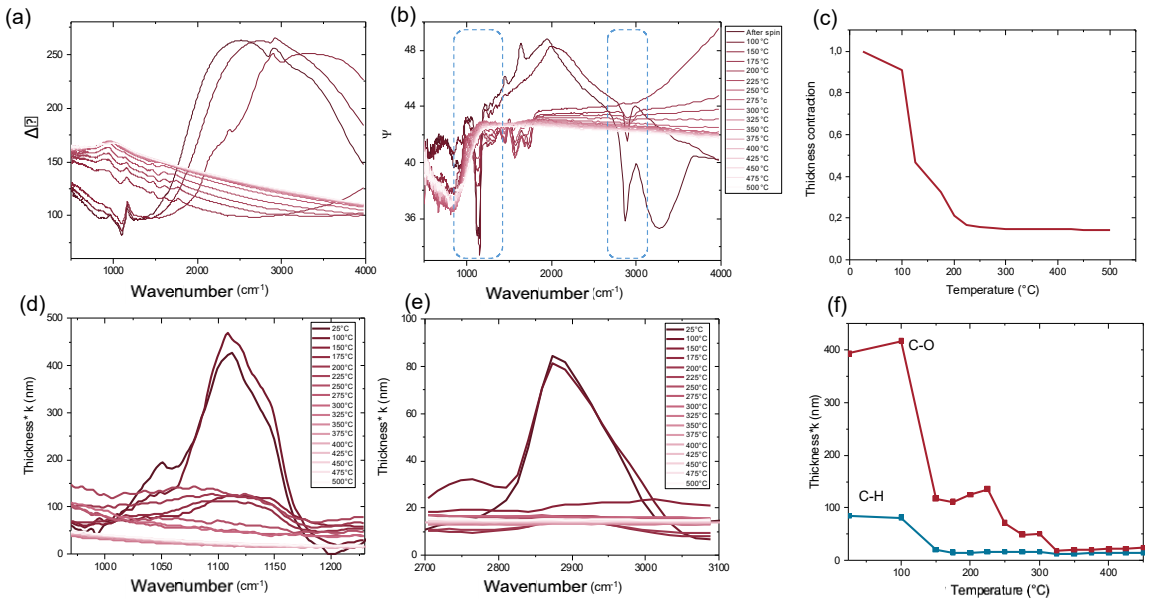


***Fig. 4*** *IR ellipsometric study of the thermal annealing. (a)* Δ and (b) Ψ experimental curves as a function of the calcination temperature *obtained by IR ellipsometry. (c) Thickness contraction as function of the temperature; k * thickness evolution for (d) C-O band and (d) C-H band. (f) Evolution of k * thickness as function of the temperature for C-O and C-H band.*

### 3.3 IR ellipsometric study of UV annealing

We then focused on the photo-annealing by using UV light. In this case, the UV treatment was performed in a separate chamber used for photopolymerization. The IR ellipsometric measurements was carried out by placing into the chamber with dried air (RH<10%) the samples annealed at increasing exposure time with a UV lamp. Figure 5 (a and b) present the evolution of Ψ and Δ curves of the film for increasing exposure times. As described above we fitted the curves to obtain thickness, n and k. The evolution of the normalized thickness as a function of the exposure time is shown in Figure 5(c). As expected, the film contracts with increasing time of exposure to UV confirming that the photo-annealing treatment has an effect on the film. The residual thickness after 20 minutes is 20% of the original thickness, a value similar to the one obtained after thermal annealing (Figure 4c). The volume loss is mainly due to block-copolymer decomposition. Figures 5(d and e) display the evolution of k multiplied by the thickness for increasing exposure time to UV light by focusing in the ranges 950-1250 and 2700-3100 $cm^{-1}$ to follow the evolution of the C-O and C-H bands respectively. Both contributions attributed to the block-copolymer progressively decrease in intensity with the exposure times, disappearing after 20 minutes. High-energy UV photons are absorbed by the absorbing species in the as-prepared coating (organic + Ti-based precursor). According to the literature[46] and similarly to X-rays[47,48], high energy UV radiation promotes the formation of free radicals, such as H° and OH°, from the residual

water molecules present in the sol–gel film. Such radicals promote the decomposition of the organic template and enhance the polycondensation kinetics of the inorganic network.[6,49-51]

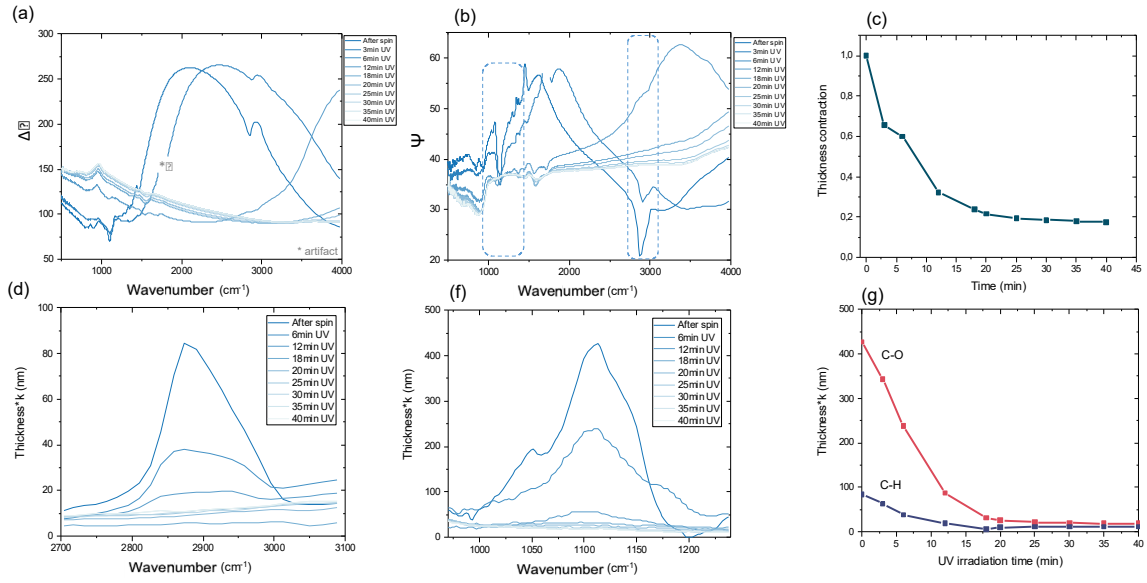


***Fig. 5*** *IR ellipsometric study of the UV annealing. (a)* Δ and (b) Ψ experimental curves as a function of the exposure time *obtained by IR ellipsometry. (c) Thickness contraction as function of the exposure time; k * thickness evolution for (d) C-O band and (d) C-H band. (f) Evolution of k * thickness as function of the exposure time for C-O and C-H bands.*

### 3.4 Complementary characterizations

The effect of the thermal- and photo- annealing on the final porosity of the films was investigated by several complementary characterization methods. The porous sorption behavior was characterized by thermo-porosimetry by in situ UV-Vis-NIR ellipsometry. The method consists of determining the evolution of the refractive index and thickness of the films as a function of the temperature in the presence of water vapor. In this configuration, the vapor atmosphere was kept at fixed relative vapor pressure $P/P_0$ = 0.5 at 20°C. Instead, the temperature of the film/substrate was varied by using a heating/cooling stage between 10 and 45°C. Since the saturated vapor pressure $P_0$ depends on the temperature, in this configuration, the local $P/P_0$ into the film can be increased and decreased by cooling or heating, respectively.[52] Water condensation and evaporation can be monitored by observing the evolution of the refractive index (at 700nm in this case). The measurements result in adsorption/desorption isobars as shows in Figure 6(b) and (d) for the heat-treated and photo-annealed films, respectively. We start the experiment at 45°C; at higher temperature the porosity is empty and the refractive index is equal to 1.59-1.60 in both cases.

Decreasing progressively the temperature to 10°C, the refractive index increases due to water capillary condensation into the mesoporous $TiO_2$. In both cases, the capillary condensation of water in the pores induces the transversal deformation that can be deduced from the thickness evolution as shown in Figure 6 (c) and (e).[34] The process is reversible; while heating, desorption occurs as testified by a decrease of the refractive index. At 10°C, the porosity is presumed to be completely filled with water. However, the refractive index of the thermally annealed films is 1.80 while that of the photo-annealed film is 1.73. This can be explained by differences in porous volume and in the nature of the inorganic wall. To gain better insights, starting from these values we evaluate the porous volume by using the Bruggeman effective medium approximation (BEMA) model (eq 1). Starting from the dielectric constant ε of the mesoporous film in the empty and full state, this model allows the determination of the dielectric constant of $TiO_2$ ($\varepsilon_T$) for both samples. In the empty and full states, the BEMA model can be written as follows:

$$f_T \frac{\tilde{\varepsilon}_T - \tilde{\varepsilon}}{\tilde{\varepsilon}_T + 2\tilde{\varepsilon}} + f_A \frac{\tilde{\varepsilon}_A - \tilde{\varepsilon}}{\tilde{\varepsilon}_A + 2\tilde{\varepsilon}} = 0 \qquad \text{empty} \qquad (1)$$

$$f_T \frac{\tilde{\varepsilon}_T - \tilde{\varepsilon}}{\tilde{\varepsilon}_T + 2\tilde{\varepsilon}} + f_W \frac{\tilde{\varepsilon}_W - \tilde{\varepsilon}}{\tilde{\varepsilon}_W + 2\tilde{\varepsilon}} = 0 \qquad \text{full} \qquad (2)$$

where $f_T$ , $f_w$ and $f_A$ and $\varepsilon_T$, $\varepsilon_W$, $\varepsilon_A$ are the relative volumetric fractions and dielectric constants of three compounds T ($TiO_2$), W (Water) and A (Air). Since air, water and $TiO_2$ do not absorb light in the considered range of wavelengths (typically 400-1000nm), the dielectric constants are taken to be the square of the refractive index values (real part of the dielectric constants). According to the scheme in Figure 6(a), all the air is replaced with water after capillary condensation. We can thus assume that:

$$f_w = f_A \qquad (3)$$

which also corresponds to the porous volume. Considering the refractive indices of water and air to be equal to 1.34 and 1, respectively, the pore volume and the $\varepsilon_T$ (and refractive index) can be calculated by combining equations (1), (2) and (3). For the thermally treated $TiO_2$ film the porous volume is around 52 % while the refractive index of the $TiO_2$ wall is 2.35, a value that is consistent with well crystallized anatase.[28] For the UV-treated sample the porous volume is 38% while the refractive index of the $TiO_2$ wall is 1.99, a value that is typical for an amorphous $TiO_2$.[36]

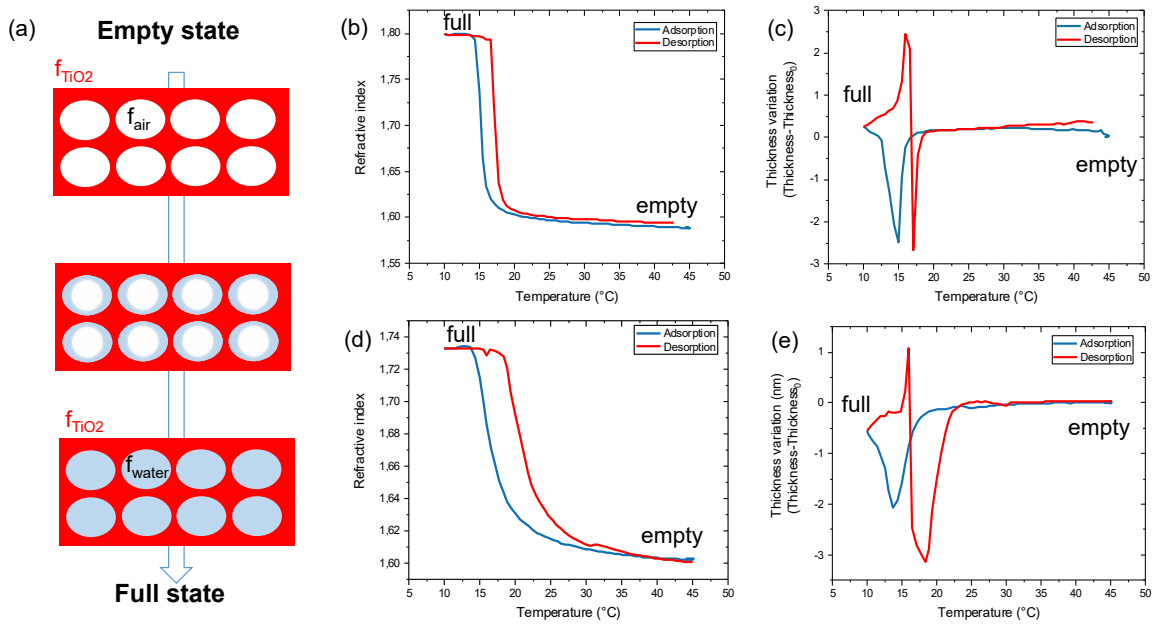


***Fig. 6*** *Ellipsometric thermo-porosimetry. Evolution of the refractive index/thickness as a function of the temperature in a closed chamber with 0.5 $P/P_0$ of water vapor for the film after (a) and (b) thermal treatment at 500°C and (c) and (d) after UV-annealing for 25 minutes.*

To gain a better understanding, the mesostructure of the films after spin-coating and after thermal or photo annealing was characterized by GISAXS (Figure 6) and SEM. After spin-coating (Figure 7a), the pattern presents diffraction features characteristic of a hybrid mesostructured film with worm-like morphology; by integrating the signal intensity, a maximum is obtained at $q_y$= 0.43 nm$^{-1}$ corresponding to a d-spacing around 14 nm which is in agreement with mesostructures containing F127 micelles. Figure 7(c) and (d) display the GISAXS patterns of the film after 10 and 40 minutes of UV exposure, respectively. Even after 10 minutes, the initial ordered mesostructure is lost. Instead, the diffused signal at lower $q_y$ suggests the presence of a larger and less ordered structure. This is confirmed by SEM as shown in Figure 6d; we choose on purpose a zone with a crack from which we can observe that the film presents a disordered porous network with polydisperse pore size. After 40 minutes (Figure 7d), more elongated patterns in the z direction of the reciprocal space are observed, indicating a higher out-of-plain contraction of the films in agreement with the ellipsometric analysis in Figure 5c. As expected, UV-treated films remain amorphous as confirmed by X-ray diffraction (XRD) in Figure S4. The effect of thermal treatment on the mesostructure is shown in Figure 7(e). After thermal treatment at 350°C, the GISAXS pattern exhibits the characteristic morphology of an open and highly accessible pseudo "grid-like" porosity, confirmed by the two parallel intense diffraction peaks of the GISAXS pattern at $q_y$ =

0.05 $nm^{-1}$ coming from the domains composed of periodical planes oriented perpendicular to the substrate. The grid-like structure results from the thermally induced transformation of the amorphous titania into a crystalline phase.[53] After thermal treatment at 500°C, sintering results in a loss of the ordering in the mesostructure as shown in Figure 7 (f) and SEM in Figure 7(g): the mesoporosity the $TiO_2$ film results from the interparticulate voids between the anatase crystals. The presence of anatase nanocrystals is confirmed by XRD in Figure S4.

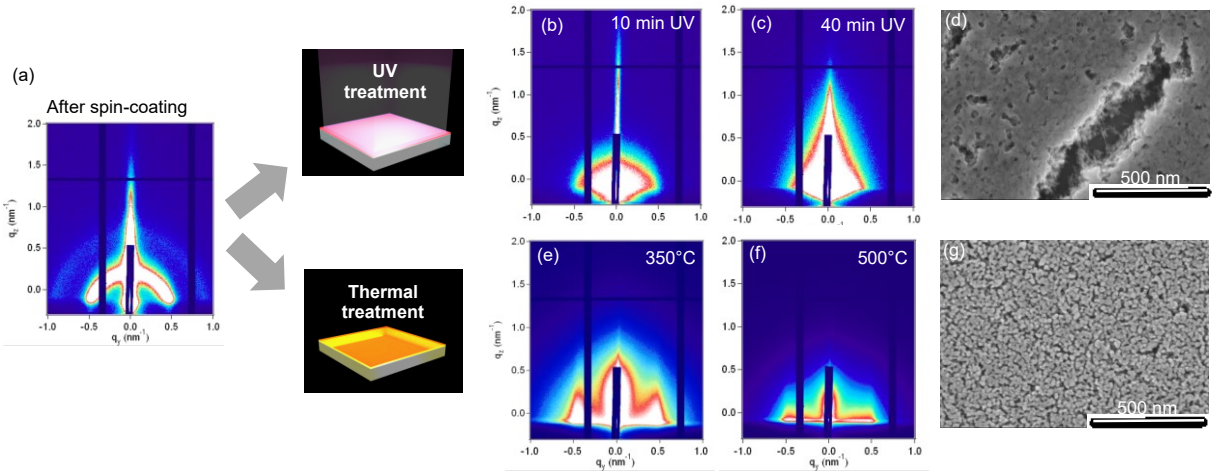


***Fig. 7*** *GISAXS study to evaluate the mesostructure of the films: (a) before annealing, by UV-annealing after (b) 10 min and (c) 40 minutes of exposure and by thermal annealing at (e) 350°C and (f) 500°C. SEM micrograph of film after (d) 25 minutes of UV annealing and (g) after thermal treatment at 500°C.*

### 3.5 Hybrid plasmonic mesoporous films

To illustrate the benefit of using a UV-annealing to obtain mesoporous $TiO_2$ films at room temperature, we have fabricated hybrid plasmonic/mesoporous films. They are made of gold bipyramids applied on a silicon substrate and covered by the thermal- or photo-annealed $TiO_2$ films. Among the various plasmonic nanoparticles, Au bipyramids have been chosen because of their superior refractive index sensitivity and figures of merit.[54] The nanoparticles have been synthetized by following protocols proposed in the literature.[55] To unveil the effect of the coating, we carried out an optical investigation of the gold nanoparticles. The scattering spectra were imaged and characterized by hyperspectral microscopy by using objectives allowing acquisition in reflection dark-field mode as shown in Figure 8a and b. The microscope is equipped with a spectrometer and a piezoelectric scanner, which moves the sample stage along the one axis to scan the surface and collect a spectrum for each pixel of a hyperspectral image.[52] The scattering spectra of two plasmonic objects in Figure 8 (c) indicate a characteristic plasmonic peak at around 660nm for both of them. This value is consistent with the fact that the plasmonic materials are

covered by a low refractive index medium ($n_{air}$=1). A large optical change occurs by covering the particles with a film heat treated at 500°C. As shown in Figure 8 (d) and (g), the scattering spectra present peaks at 545 nm indicating that the Au bipyramids have been reshaped into spheres. Indeed, it is well established that heat treatment induces reshaping of plasmonic anisotropic nanoparticle at relatively low temperature.[56,57] The particles covered by UV-annealed films are displayed in Figure 8 (d) and (g): the scattering spectra show plasmonic peaks that are centered at 725 nm. The red-shift is consistent with the fact that the mesoporous layer has a refractive index higher than air (around 1.6 according to Figure 6c). More importantly, this behavior confirms that the room-temperature UV-annealing does not provoke a significant deformation of the Au bipyramids as in the case of thermal annealing that is of interest for sensing application for instance.

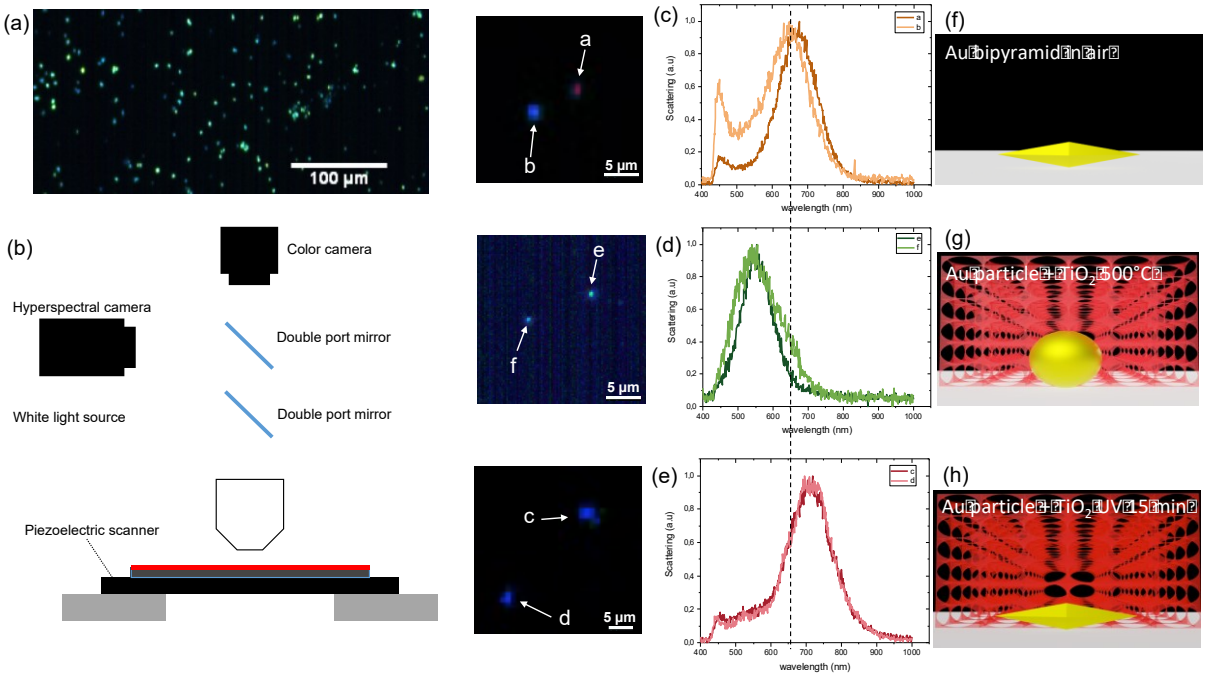


***Fig. 8*** *Hyperspectral microscopy analysis of plasmonic particles covered with $TiO_2$ based films. (a) Dark field micrograph of Au bipyramids on silicon. (b) Illustration of the hyperspectral microscope set-up. Hyperspectral images and corresponding scattering curves of the plasmonic particles (c) in air, (d) covered with a $TiO_2$ layer heat treated at 500°C and (f) covered with a UV-annealed $TiO_2$ layer. The dotted line is a guide for the eye. (f), (g) and (h) are illustrations of the corresponding proposed systems.*

**4) Discussion**

At the current stage, this technique presents advantages and drawbacks with respect to the most commonly employed UV-vis-NIR ellipsometry.[26] We summarize these features in Table 1. Both spectroscopic ellipsometries are well suited to follow structural changes on the

films (contraction, volume loss) and the evolution of the optical properties in the respective spectral ranges. In addition to these features, the main advantage of IR ellipsometry is that it provides direct information about the chemical evolution of the films. Depending on the objective of the investigation, the Ψ and Δ curves obtained from IR ellipsometry can be further analyzed and fitted by employing approaches with different levels of complexity. The presence or absence of a certain chemical species can be determined qualitatively directly from the raw Ψ and Δ curves. For in situ studies, this is particularly appropriate for identifying reaction intermediates. [58]

| | UV-vis-NIR ellipsometry | IR ellipsometry |
|---|---|---|
| *Structural evolution* | +++ | +++ |
| *Optical properties* | +++ | +++ |
| *Chemical evolution* | - | +++ |
| *Time resolved experiments* | +++ | + |

***Table 1*** *Advantages and drawbacks of UV-vis-NIR ellipsometry and IR ellipsometry*

Quantitative characterization of the vibrational bands requires development of rigorous fitting procedures, especially in the case of time-resolved experiments. In certain cases, if the absorption bands are well resolved, they can be fitted by Lorentz oscillators to deconvolute each vibrational mode.[59] This possibility strongly depends on the quality of the measurement and thus on the acquisition time. Indeed, as summarized in Table 1, the acquisition time remains the main limitation of IR ellipsometry for in situ experiments. In the conventional UV-vis-NIR ellipsometry, the measurement is fast (below one second) making it perfectly suited to investigating phenomena with characteristic times above tens of seconds. In the case of IR ellipsometry, while a basic measurement can be made in only a few minutes, obtaining high quality spectra can require up to several tens of minutes (depending on the systems). This can represent a limitation for in situ experiments aiming at studying fast phenomena. Summarizing, with the current technology, the two instruments provide complementary advantages. Designing combined studies coupling UV-vis-NIR ellipsometry and IR ellipsometry represents an ideal strategy to characterize sol-gel films by taking advantage of both techniques.

## 5) Conclusions

In conclusion, in this article, we expand the available toolbox[23] to probe the formation of sol-gel derived mesoporous films by introducing IR ellipsometry as a multiparameter method. We investigated two annealing methods to obtain mesoporous $TiO_2$ films. Interestingly, UV-annealing allows fabrication of mesoporous $TiO_2$ films at low temperature that make it a valuable method to couple sol-gel films with temperature sensitive materials such as plasmonic nanoparticles. More broadly, this work represents one of first attempts to apply in situ IR ellipsometry to characterize the evolution of sol-gel materials. This in situ methodology can be extended to other functional materials and devices beyond sol-gel oxides, such as perovskite solar cell, organic electronics or metallic metasurfaces.

**Funding Sources**

This work was supported by the European Research Council (ERC) under European Union's Horizon 2020 Programme (Grant Agreement no. 803220, TEMPORE). This project has also received funding from the EU-H2020 research and innovation programme under grant agreement No. 654360 having benefitted from the access provided by ELETTRA Trieste, Italy, within the framework of the NFFA-Europe Transnational Access Activity. The infrared ellipsometry was funded by the Région Ile-de-France in the framework of DIM ResPore and by the French state within the Investissements d'Avenir programme under reference ANR-11-IDEX-0004-02, within the framework of the Cluster of Excellence MATISSE.

**Acknowledgment**

We thank D. Montero and the Institut des Matériaux de Paris Centre (IMPC FR2482) for servicing FEGSEM & EDX instrumentation and Sorbonne Université, CNRS and C'Nano projects of the Région Ile-de-France for funding.

**Compliance with ethical standards**

Conflict of interest The authors declare no competing interests.

**References**

1. Sanchez C, Julian B, Belleville P, Popall M (2005) Applications of hybrid organic-inorganic nanocomposites. Journal of Materials Chemistry 15 (35-36):3559-3592. doi:10.1039/B509097K
2. Faustini M, Nicole L, Boissiere C, Innocenzi P, Sanchez C, Grosso D (2010) Hydrophobic, Antireflective, Self-Cleaning, and Antifogging Sol-Gel Coatings: An Example of Multifunctional Nanostructured Materials for Photovoltaic Cells. Chemistry of Materials 22 (15):4406-4413. doi:10.1021/cm100937e
3. Pénard A-L, Gacoin T, Boilot J-P (2007) Functionalized Sol–Gel Coatings for Optical Applications. Accounts of Chemical Research 40 (9):895-902. doi:10.1021/ar600025j

4. Odziomek M, Thorimbert F, Boissiere C, Drisko GL, Parola S, Sanchez C, Faustini M (2022) Periodic Nanoporous Inorganic Patterns Directly Made by Self - Ordering of Cracks. Adv Mater 34 (36):2204489
5. Li R, Boudot M, Boissière C, Grosso D, Faustini M (2017) Suppressing Structural Colors of Photocatalytic Optical Coatings on Glass: The Critical Role of SiO2. ACS Applied Materials & Interfaces 9 (16):14093-14102. doi:10.1021/acsami.7b02233
6. Faustini M, Grenier A, Naudin G, Li R, Grosso D (2015) Ultraporous nanocrystalline TiO2-based films: synthesis, patterning and application as anti-reflective, self-cleaning, superhydrophilic coatings. Nanoscale 7 (46):19419-19425. doi:10.1039/C5NR06466J
7. Grosso D, Boissière C, Sanchez C (2007) Ultralow-dielectric-constant optical thin films built from magnesium oxyfluoride vesicle-like hollow nanoparticles. Nature materials 6 (8):572-575
8. Gayrard M, Voronkoff J, Boissière C, Montero D, Rozes L, Cattoni A, Péron J, Faustini M (2021) Replacing Metals with Oxides in Metal-Assisted Chemical Etching Enables Direct Fabrication of Silicon Nanowires by Solution Processing. Nano Letters 21 (5):2310-2317
9. Neu V, Schulze C, Faustini M, Lee J, Makarov D, Suess D, Kim SK, Grosso D, Schultz L, Albrecht M (2013) Probing the energy barriers and magnetization reversal processes of nanoperforated membrane based percolated media. Nanotechnology 24 (14). doi:10.1088/0957-4484/24/14/145702
10. Faustini M, Drisko GL, Letailleur AA, Montiel RS, Boissiere C, Cattoni A, Haghiri-Gosnet AM, Lerondel G, Grosso D (2013) Self-assembled titanium calcium oxide nanopatterns as versatile reactive nanomasks for dry etching lithographic transfer with high selectivity. Nanoscale 5 (3):984-990. doi:10.1039/c2nr33341d
11. Grobis M, Schulze C, Faustini M, Grosso D, Hellwig O, Makarov D, Albrecht M (2011) Recording study of percolated perpendicular media. Applied Physics Letters 98 (19). doi:10.1063/1.3587635
12. Cattoni A, Mailly D, Dalstein O, Faustini M, Seniutinas G, Rösner B, David C (2018) Sub-10 nm electron and helium ion beam lithography using a recently developed alumina resist. Microelectronic Engineering 193:18-22
13. Orilall MC, Wiesner U (2011) Block copolymer based composition and morphology control in nanostructured hybrid materials for energy conversion and storage: solar cells, batteries, and fuel cells. Chemical Society Reviews 40 (2):520-535. doi:10.1039/C0CS00034E
14. Ceratti DR, Louis B, Paquez X, Faustini M, Grosso D (2015) A New Dip Coating Method to Obtain Large-Surface Coatings with a Minimum of Solution. Adv Mater 27 (34):4958-+. doi:10.1002/adma.201502518
15. Elmaalouf M, Odziomek M, Duran S, Gayrard M, Bahri M, Tard C, Zitolo A, Lassalle-Kaiser B, Piquemal J-Y, Ersen O, Boissière C, Sanchez C, Giraud M, Faustini M, Peron J (2021) The origin of the high electrochemical activity of pseudo-amorphous iridium oxides. Nature Communications 12 (1):3935. doi:10.1038/s41467-021-24181-x
16. De Marco ML, Baaziz W, Sharna S, Devred F, Poleunis C, Chevillot-Biraud A, Nowak S, Haddad R, Odziomek M, Boissière C, Debecker DP, Ersen O, Peron J, Faustini M (2022) High-Entropy-Alloy Nanocrystal Based Macro- and Mesoporous Materials. ACS Nano 16 (10):15837-15849. doi:10.1021/acsnano.2c05465
17. Boudot M, Cattoni A, Grosso D, Faustini M (2016) Ethanol–water co-condensation into hydrophobic mesoporous thin films: example of a photonic ethanol vapor sensor in humid environment. Journal of Sol-Gel Science and Technology:1-10. doi:10.1007/s10971-016-4084-2
18. Carboni D, Jiang Y, Faustini M, Malfatti L, Innocenzi P (2016) Improving the selective efficiency of graphene-mediated enhanced Raman scattering through molecular imprinting. ACS Applied Materials & Interfaces
19. Innocenzi P, Malfatti L (2013) Mesoporous thin films: properties and applications. Chemical Society Reviews 42 (9):4198-4216. doi:10.1039/C3CS35377J

20. Sanchez C, Boissière C, Grosso D, Laberty C, Nicole L (2008) Design, synthesis, and properties of inorganic and hybrid thin films having periodically organized nanoporosity. Chem Mat 20 (3):682-737
21. Seco AM, Gonçalves MC, Almeida RM (2000) Densification of hybrid silica–titania sol–gel films studied by ellipsometry and FTIR. Materials Science and Engineering: B 76 (3):193-199. doi:https://doi.org/10.1016/S0921-5107(00)00442-6
22. Innocenzi P, Malfatti L, Kidchob T, Costacurta S, Falcaro P, Piccinini M, Marcelli A, Morini P, Sali D, Amenitsch H (2007) Time-Resolved Simultaneous Detection of Structural and Chemical Changes during Self-Assembly of Mesostructured Films. The Journal of Physical Chemistry C 111 (14):5345-5350. doi:10.1021/jp066566c
23. Alvarez-Fernandez A, Reid B, Fornerod MJ, Taylor A, Divitini G, Guldin S (2020) Structural Characterization of Mesoporous Thin Film Architectures: A Tutorial Overview. ACS Applied Materials & Interfaces 12 (5):5195-5208. doi:10.1021/acsami.9b17899
24. Hurd AJ, Brinker CJ (1988) Optical sol-gel coatings: ellipsometry of film formation. Journal de Physique 49 (6):1017-1025
25. Xie H, Wei J, Zhang X Characterisation of sol-gel thin films by spectroscopic ellipsometry. In: Journal of Physics: Conference Series, 2006. IOP Publishing, p 020
26. Gartner M, Stoica M, Nicolescu M, Stroescu H (2021) The ellipsometry versatility in the study of sol-gel films. JOURNAL OF SOL-GEL SCIENCE AND TECHNOLOGY 98 (1):1-23. doi:10.1007/s10971-021-05504-2
27. Boudot M, Ceratti DR, Faustini M, Boissiere C, Grosso D (2014) Alcohol-Assisted Water Condensation and Stabilization into Hydrophobic Mesoporosity. Journal of Physical Chemistry C 118 (41):23907-23917. doi:10.1021/jp508372d
28. Louis B, Krins N, Faustini M, Grosso D (2011) Understanding Crystallization of Anatase into Binary SiO2/TiO2 Sol-Gel Optical Thin Films: An in Situ Thermal Ellipsometry Analysis. Journal of Physical Chemistry C 115 (7):3115-3122. doi:10.1021/jp109653p
29. Li R, Faustini M, Boissiere C, Grosso D (2014) Water Capillary Condensation Effect on the Photocatalytic Activity of Porous TiO2 in Air. Journal of Physical Chemistry C 118 (31):17710-17716. doi:10.1021/jp5046468
30. Bindini E, Chehadi Z, Faustini M, Albouy P-A, Grosso D, Cattoni A, Chanéac C, Azzaroni O, Sanchez C, Boissière C (2020) Following in Situ the Degradation of Mesoporous Silica in Biorelevant Conditions: At Last, a Good Comprehension of the Structure Influence. ACS Applied Materials & Interfaces 12 (12):13598-13612. doi:10.1021/acsami.9b19956
31. Dalstein O, Ceratti DR, Boissière C, Grosso D, Cattoni A, Faustini M (2016) Nanoimprinted, Submicrometric, MOF - Based 2D Photonic Structures: Toward Easy Selective Vapors Sensing by a Smartphone Camera. Advanced Functional Materials 26 (1):81-90
32. Löbmann P (2017) Characterization of sol–gel thin films by ellipsometric porosimetry. Journal of Sol-Gel Science and Technology 84 (1):2-15
33. Baklanov bMR, Mogilnikov KP, Polovinkin VG, Dultsev FN (2000) Determination of pore size distribution in thin films by ellipsometric porosimetry. Journal of Vacuum Science & Technology B: Microelectronics and Nanometer Structures Processing, Measurement, and Phenomena 18 (3):1385-1391
34. Boissiere C, Grosso D, Lepoutre S, Nicole L, Bruneau AB, Sanchez C (2005) Porosity and Mechanical Properties of Mesoporous Thin Films Assessed by Environmental Ellipsometric Porosimetry. Langmuir 21 (26):12362-12371. doi:10.1021/la050981z
35. Bruynooghe S, Bertin F, Chabli A, Gay JC, Blanchard B, Couchaud M (1998) Infrared spectroscopic ellipsometry for residual water detection in annealed sol–gel thin layers. Thin Solid Films 313-314:722-726. doi:https://doi.org/10.1016/S0040-6090(97)00985-1
36. Bass JD, Grosso D, Boissiere C, Sanchez C (2008) Pyrolysis, Crystallization, and Sintering of Mesostructured Titania Thin Films Assessed by in Situ Thermal Ellipsometry. Journal of the American Chemical Society 130 (25):7882-7897. doi:10.1021/ja078140x
37. Amenitsch H, Rappolt M, Kriechbaum M, Mio H, Laggner P, Bernstorff S (1998) First performance assessment of the small-angle X-ray scattering beamline at ELETTRA. Journal of synchrotron radiation 5 (3):506-508

38. Soler-Illia GJAA, Angelomé PC, Fuertes MC, Grosso D, Boissiere C (2012) Critical aspects in the production of periodically ordered mesoporous titania thin films. Nanoscale 4 (8):2549-2566
39. Crepaldi EL, Soler-Illia GJdAA, Grosso D, Cagnol F, Ribot F, Sanchez C (2003) Controlled Formation of Highly Organized Mesoporous Titania Thin Films: From Mesostructured Hybrids to Mesoporous Nanoanatase TiO2. Journal of the American Chemical Society 125 (32):9770-9786. doi:10.1021/ja030070g
40. Joel M, Thomas ET, Jeffrey SH, James NH, Andrew CM (2020) Application of a B-spline model dielectric function to infrared spectroscopic ellipsometry data analysis. Journal of Vacuum Science & Technology B 38 (1):014001. doi:10.1116/1.5126110
41. Silverstein RM, Bassler GC (1962) Spectrometric identification of organic compounds. Journal of Chemical Education 39 (11):546
42. Pielichowski K, Flejtuch K (2005) Non-oxidative thermal degradation of poly (ethylene oxide): kinetic and thermoanalytical study. Journal of Analytical and Applied Pyrolysis 73 (1):131-138
43. Innocenzi P, Kidchob T, Costacurta S, Falcaro P, Marmiroli B, Cacho-Nerin F, Amenitsch H (2010) Patterning block copolymer thin films by deep X-ray lithography. Soft Matter 6 (14):3172-3176
44. de Sainte Claire P (2009) Degradation of PEO in the Solid State: A Theoretical Kinetic Model. Macromolecules 42 (10):3469-3482. doi:10.1021/ma802469u
45. Malfatti L, Falcaro P, Amenitsch H, Caramori S, Argazzi R, Bignozzi CA, Enzo S, Maggini M, Innocenzi P (2006) Mesostructured self-assembled titania films for photovoltaic applications. Microporous and Mesoporous Materials 88 (1):304-311. doi:https://doi.org/10.1016/j.micromeso.2005.09.027
46. Brigo L, Grenci G, Carpentiero A, Pistore A, Tormen M, Guglielmi M, Brusatin G (2011) Positive resist for UV and X-ray lithography synthesized through sol–gel chemistry. J Sol-Gel Sci Technol 60 (3):400-407. doi:10.1007/s10971-011-2512-x
47. Faustini M, Marmiroli B, Malfatti L, Louis B, Krins N, Falcaro P, Grenci G, Laberty-Robert C, Amenitsch H, Innocenzi P, Grosso D (2011) Direct nano-in-micropatterning of TiO2 thin layers and TiO2/Pt nanoelectrode arrays by deep X-ray lithography. Journal of Materials Chemistry 21 (11):3597-3603. doi:10.1039/c0jm03493b
48. Falcaro P, Malfatti L, Vaccari L, Amenitsch H, Marmiroli B, Grenci G, Innocenzi P (2009) Fabrication of Advanced Functional Devices Combining Soft Chemistry with X-ray Lithography in One Step. Advanced Materials 21 (48):4932-+. doi:10.1002/adma.200901561
49. Gómez-Lopez A, Rivas YA, López-Fajardo S, Jiménez R, Ricote J, Pecharromán C, Montero I, Bretos I, Calzada ML (2023) In situ photogenerated hydroxyl radicals in the reaction atmosphere for the accelerated crystallization of solution-processed functional metal oxide thin films. Journal of Materials Chemistry C 11 (7):2619-2629. doi:10.1039/D2TC05447G
50. Bretos I, Jiménez R, Ricote J, Calzada ML (2020) Photochemistry in the low - temperature processing of metal oxide thin films by solution methods. Chemistry–A European Journal 26 (42):9277-9291
51. De Dobbelaere C, Calzada ML, Jiménez R, Ricote J, Bretos I, Mullens J, Hardy A, Van Bael MK (2011) Aqueous Solutions for Low-Temperature Photoannealing of Functional Oxide Films: Reaching the 400 °C Si-Technology Integration Barrier. Journal of the American Chemical Society 133 (33):12922-12925. doi:10.1021/ja203553n
52. Avci C, De Marco ML, Byun C, Perrin J, Scheel M, Boissière C, Faustini M (2021) Metal–organic framework photonic balls: single object analysis for local thermal probing. Adv Mater 33 (43):2104450
53. Grosso D, Soler-Illia GJdAA, Crepaldi EL, Cagnol F, Sinturel C, Bourgeois A, Brunet-Bruneau A, Amenitsch H, Albouy PA, Sanchez C (2003) Highly Porous TiO2 Anatase Optical Thin Films with Cubic Mesostructure Stabilized at 700 °C. Chemistry of Materials 15 (24):4562-4570. doi:10.1021/cm031060h
54. Chen H, Kou X, Yang Z, Ni W, Wang J (2008) Shape- and Size-Dependent Refractive Index Sensitivity of Gold Nanoparticles. Langmuir 24 (10):5233-5237. doi:10.1021/la800305j

55. Chateau D, Desert A, Lerouge F, Landaburu G, Santucci S, Parola S (2019) Beyond the Concentration Limitation in the Synthesis of Nanobipyramids and Other Pentatwinned Gold Nanostructures. ACS Applied Materials & Interfaces 11 (42):39068-39076. doi:10.1021/acsami.9b12973
56. Wang Y, Teitel S, Dellago C (2005) Surface-driven bulk reorganization of gold nanorods. Nano letters 5 (11):2174-2178
57. Opletal G, Grochola G, Chui YH, Snook IK, Russo SP (2011) Stability and Transformations of Heated Gold Nanorods. The Journal of Physical Chemistry C 115 (11):4375-4380. doi:10.1021/jp1074913
58. Gayrard M, Chancerel F, De Marco ML, Naumenko D, Boissière C, Rozes L, Amenitsch H, Peron J, Cattoni A, Faustini M (2022) Block-Copolymers Enable Direct Reduction and Structuration of Noble Metal-Based Films. Small 18 (5):2104204. doi:https://doi.org/10.1002/smll.202104204
59. Dasgupta S, Biswas S, Dedecker K, Dumas E, Menguy N, Berini B, Lavedrine B, Serre C, Boissière C, Steunou N (2023) In Operando Spectroscopic Ellipsometry Investigation of MOF Thin Films for the Selective Capture of Acetic Acid. ACS Applied Materials & Interfaces. doi:10.1021/acsami.2c17682